Simulation of Jets with a Finite Element Navier-Stokes Solver and a Multilevel VOF Approach

A. Cervone, S. Manservisi* and R. Scardovelli
DIENCA, Laboratorio di Montecuccolino, Università di Bologna
Via dei Colli 16, 40136 Bologna, Italy

Abstract

An accurate finite element Navier-Stokes solver is presented to simulate axis-symmetric and three-dimensional incompressible jets. It is based on a multilevel approach where the Volume-of-Fluid (VOF) scalar function is defined on a high resolution grid and then is projected on a coarser grid where the velocity field is computed. With this approach it is possible to consider grid spacings that ensure a high value of the ratio between the local radius of the interface curvature and the cell size even for three-dimensional computational domains. Since the number of cut cells is usually much smaller than the total number of cells in the computational domain, we have implemented a compact memorization of the VOF data based on a sparse matrix storage approach. In order to prove the validity of this numerical method we have computed the growth rate of several linear instability modes of a viscous liquid jet surrounded by a gas and compared them to the analytical results for inviscid fluids derived in axis-symmetric geometry. A number of jet simulations with a sinusoidal oscillation of the inlet velocity are presented. At low Weber and Reynolds numbers the simulations are axis-symmetric and we show the time evolution of drops, threads and satellite droplets. At higher Weber numbers, with $We > We_c$, asymmetric modes are excited and the jet evolution is followed with the three-dimensional version of the model.

Introduction

A stream of liquid matter that enters a gas region and breaks into small liquid masses is a very complex phenomenon that occurs in many natural and engineering processes. Many type of engines require injections of fluid and gas streams as essential part of the combustion process or as primary coolant for heat removal. Liquid jets are also used to test free-surface motions, hydrodynamic instabilities and singular formations that lead to drop breakup and coalescence. However, jet dynamics is very sensitive to boundary conditions, to the turbulent status of the fluid and to the surrounding gas and the mechanisms leading to small fluid structures and droplets are still open questions and objective of active research. In recent time, many studies have investigated jets with direct numerical simulations, by using Volume-of-Fluid [1], Level Set [2] and Front Tracking methods [3] to represent the interface. In this paper we propose a multilevel VOF computation associated with a finite element solver that can in part reduce the problems related to the automatic merging and breakup of interfaces, the computation of capillary forces and the generation of spurious currents. The interface is defined on a very refined grid, while the velocity field is computed on a coarser grid. The interface advection and the capillary force computation are performed on the refined grid, reducing the arbitrary breakup and the errors in the force balance at the interface. Several test examples are presented to show the accuracy and robustness of the proposed scheme.

Navier-Stokes Equations, Variational Formulation and Finite Element Discretization

We consider a computational domain $\Omega \subset R^3$ with boundary Γ. The liquid (reference) phase is located in $\Omega_l(t) \subset \Omega$ with boundary Γ_l and completely surrounded by a gas (secondary) phase filling the domain $\Omega_g(t) = \Omega - \Omega_l(t)$. The interface between the two immiscible fluids is denoted by $\Gamma_s \subset \Gamma_l$. The distribution of the liquid in Ω_l is defined by the characteristic function $\chi(\mathbf{x}, t)$ which is one for all $\mathbf{x} \in \Omega_l$ and zero on $\Omega - \Omega_l$. Across the interface the function χ is discontinuous. Since each fluid parcel does not change its identity, the indicator χ satisfies a simple advection equation

$$\frac{\partial \chi}{\partial t} + (\mathbf{u} \cdot \nabla)\chi = 0\,. \tag{1}$$

The velocity $\mathbf{u}$ and pressure p obey the single-fluid formulation of the Navier-Stokes equations over the whole domain

*Corresponding author, sandro.manservisi@mail.ing.unibo.it

Ω, given by the momentum conservation equation,

$$\rho \frac{\partial \mathbf{u}}{\partial t} + (\mathbf{u} \cdot \nabla)\mathbf{u} = -\nabla p + \nabla \cdot (2\mu \mathbf{D}) + \mathbf{F} + \mathbf{F}_s \,, \tag{2}$$

and the incompressibility constraint, $\nabla \cdot \mathbf{u} = 0$. In our model each phase has constant physical properties so that the density ρ and viscosity μ in (2) are only functions of the indicator χ, i.e. $\rho = \chi\rho_l + (1-\chi)\rho_g$ and $\mu = \chi\mu_l + (1-\chi)\mu_g$. In (2) the rate-of-strain tensor $\mathbf{D}(\mathbf{u})$ is defined by $2D_{ij} = (\partial u_i/\partial x_j + \partial u_j/\partial x_i)$. The external body force is only gravity, $\mathbf{F} = \rho\mathbf{g}$, and the interfacial force acting on Γ_s is limited to capillarity [4]

$$\mathbf{F}_s(\mathbf{x}) = -\int_{\Gamma_s} \sigma\kappa\,\mathbf{n}\,\delta(\mathbf{x} - \mathbf{x}_s)\,ds \,, \tag{3}$$

where $\mathbf{x}_s$ are points on Γ_s, σ is the constant surface tension coefficient, $\mathbf{n}$ the unit external normal, κ the interface mean curvature and $\delta(\mathbf{x})$ the volumetric Dirac delta function. The normal $\mathbf{n}$, the mean curvature κ and the interface Γ_s are all geometrical quantities that can be evaluated from a given χ distribution. For simplicity, we consider Dirichlet boundary conditions at the inlet Γ_i and homogeneous Neumann boundary conditions at the outlet Γ_o.

Since the Navier-Stokes equations are not always properly defined in standard functional spaces due to the presence of distributions and derivatives of discontinuous functions we introduce the problem in variational form. Of special interest are the space $\mathbf{H}^1(\Omega)$ of vector-valued functions with each component having square integrable first derivative over Ω and the space $L^2_0(\Omega)$ of square integrable functions having zero mean over Ω. With this notation we introduce the following continuous bilinear and trilinear forms

$$a(\mu, \mathbf{u}, \mathbf{v}) = 2\int_\Omega \mu\,\mathbf{D}(\mathbf{u}) : \mathbf{D}(\mathbf{v})\,dV \,; \quad b(q, \mathbf{v}) = -\int_\Omega q\,\nabla \cdot \mathbf{v}\,dV \,; \quad c(\rho, \mathbf{w}, \mathbf{u}, \mathbf{v}) = \int_\Omega \rho\,(\mathbf{w} \cdot \nabla)\mathbf{u} \cdot \mathbf{v}\,dV \,, \tag{4}$$

where the density ρ and the viscosity μ are positive functions in Ω, $q \in L^2_0(\Omega)$ and $\mathbf{w}, \mathbf{u}, \mathbf{v} \in \mathbf{H}^1(\Omega)$. For $\Gamma_i \subset \Gamma$ with nonzero measure, we also consider the subspace of functions $\mathbf{H}^1_{\Gamma_i}(\Omega) \subset \mathbf{H}^1(\Omega)$, which vanish on Γ_i.

The weak form of the two-phase momentum equation, can be obtained by multiplying (2) with the test functions $\mathbf{v} \in \mathbf{H}^1_{\Gamma_i}(\Omega)$ and integrating over the domain Ω

$$(\rho\frac{\partial \mathbf{u}}{\partial t}, \mathbf{v}) + c(\rho, \mathbf{u}, \mathbf{u}, \mathbf{v}) - b(p, \mathbf{v}) = a(\mu, \mathbf{u}, \mathbf{v}) + (\mathbf{F}, \mathbf{v}) + (\mathbf{F}_s, \mathbf{v}) \tag{5}$$

and similarly for the incompressibility constraint, $b(q, \mathbf{u}) = 0$, with $q \in L^2_0(\Omega)$ [5]. To evaluate the interface integral, we first replace the curvature term by the Laplace–Beltrami operator $\nabla_s = (I - \mathbf{nn}) \cdot \nabla$ [6] and then integrate by parts on the interface Γ_s to obtain

$$(\mathbf{F}_s, \mathbf{v}) = -\int_{\Gamma_s} \sigma\kappa\mathbf{n} \cdot \mathbf{v}\,ds = -\int_{\Gamma_s} \sigma\nabla^2_s\,\mathbf{x}_s \cdot \mathbf{v}\,ds = \int_{\Gamma_s} \sigma\nabla_s\mathbf{x}_s : \nabla_s\mathbf{v}\,ds \,, \tag{6}$$

where we have used the relation $\kappa\,\mathbf{n} = \nabla^2_s\,\mathbf{x}_s$. Since we consider only closed interfaces or open interfaces coupled with Dirichlet boundary conditions, no additional integrals over the boundary of the interface appear.

To solve numerically (5) we seek solutions in families of finite element spaces and we introduce a finite element discretization of the Cartesian domain Ω through the mesh parameter h which tends to zero. We subdivide Ω into a family of squares of side h in axis-symmetric geometry and a family of cubes of side h in three dimensions which obey the finite element compatibility constraints on their boundary. Let $\mathbf{X}^h \subset \mathbf{H}^1(\Omega)$ and $S^h \subset L^2_0(\Omega)$ be two families of finite dimensional subspaces parameterized by the length h. We make the usual approximation assumptions on X^h and S^h, including the *inf-sup* or LBB condition (see, e.g., [7], and use standard quadrangular and hexahedric isoparametric Taylor-Hood elements. In the remaining of the paper, we will always consider these finite element spaces and suppress the h superscript.

Multilevel Approach

Let us consider a two-level solution scheme where a fine level solution (f) and a coarse level one (c) can be defined. At the fine level the advection equation is solved geometrically for the VOF function C^f, which represents

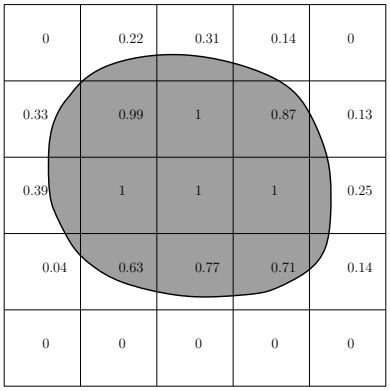

row	n_c	C					column				
1	3	0.22	0.31	0.14			2	3	4		
2	5	0.33	0.99	1	0.87	0.13	1	2	3	4	5
3	3	0.39	3	0.25			1	2	5		
4	5	0.04	0.63	0.77	0.71	0.14	1	2	3	4	5
5	0										

Figure 1: The C data distribution on a 5×5 cartesian mesh (left) and the stored data (right), including the row number, the number of cells n_c, the color function in the mixed and consecutive full cells and the column position.

the fraction of each computational cell occupied by the reference phase. At the coarse level only large phase structures are considered and (5) is solved for the pressure and velocity fields. In our formulation, the dynamics is supposed to be correctly resolved at the coarse level, while the phase structure described by the C data at the fine level is integrated at the coarse level via level transfer operators. Starting from the solution at both levels and by assuming that any test function at the coarse level can be represented as a linear combination of the test functions at the fine level, we obtain for the coarse grid solution

$$(\rho \frac{\partial \mathbf{u}}{\partial t}, \mathbf{v}) + c(\rho, \mathbf{u}, \mathbf{u}, \mathbf{v}) - b(p, \mathbf{v}) + a(\mu, \mathbf{u}, \mathbf{v}) = (\mathbf{F}, \mathbf{v}) + (\mathbf{F}_s^f, \mathbf{v}) + (R^{cf}(p, p^f, \mathbf{u}, \mathbf{u}^f), \mathbf{v}), \tag{7}$$

where variables with no superscript are defined at the coarse level and R^{cf} is the momentum transfer operator. In this paper, the operator R^{cf} is assumed to be small and is simply neglected.

The multilevel VOF method advances in time on a cartesian grid the C data at the fine level (f) and then projects the resulting color function C^f and the surface tension force $\mathbf{F}_s^f$ on the coarse level (c) where the pressure and velocity fields are computed. As we resolve more accurately the interface from the coarse level by subdividing subsequently the cells with the midpoint rule, the number of cut cells increases roughly only linearly with the level of refinement and the computational overhead due to this approach is still negligible when compared to the multigrid solver of the momentum equation. However, it would require a considerable amount of memory space to store the full matrix of the C^f data, in particular for three-dimensional computations. Since the spatial distribution of the C field changes in time, all the entries of the color function matrix must be available and this requires also the storage of empty and full cells which may become mixed cells at some later time in the simulation. In this paper we propose a multilevel storage scheme which memorizes the whole matrix of the color function at the coarse level (c), so that density and viscosity can be computed at this level, but only sparse data at the fine level (f), implementing in this way the storage of the interface data alone at each time step. This allows us to compute the color function distribution over a highly-refined mesh with an accuracy and efficiency comparable to an adaptive mesh refinement method. The sparse storage pattern is very simple. We illustrate this technique in two dimensions in Fig. 1 by considering a $[5 \times 5]$ cartesian mesh with the corresponding C data. The extension to three dimensions is straightforward. For each row we store the number of entries n_c, the C data and their column number. Notice that empty cells are not stored, while a sequence of n consecutive full cells is stored as a single one, with its color function value equal to n in the first internal cell position. For example in the third row of Fig. 1 we have three consecutive full cells, hence $C = 3$, with the first one in the second column. With this technique we can describe interfaces on a very refined mesh while the storage requirements are proportional to the fluid body surface divided by that of the cell face. This representation requires an efficient numerical algorithm to extract and compress data in the compact sparse matrix representation. In Fig. 2 we show the whole color function matrix at the coarse level (c), here with 16 cells along each coordinate direction, and the sparse color function matrices at the two levels $f = c + 2$ and $f = c + 4$. At the intermediate level of refinement each cell of the coarse grid is divided in 16 subcells with the interface clearly marked on the grid. At the highest level of refinement each coarse cell is subdivided into 256 smaller cells, with matrix entries about 16 times those of the coarse

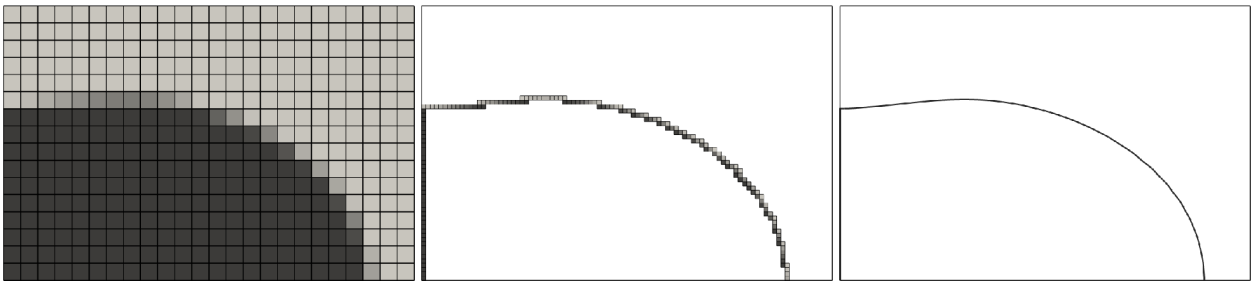

Figure 2: The C data distribution on a coarse mesh (left) and the compact data memorization with two (center) and four (right) levels of grid refinement.

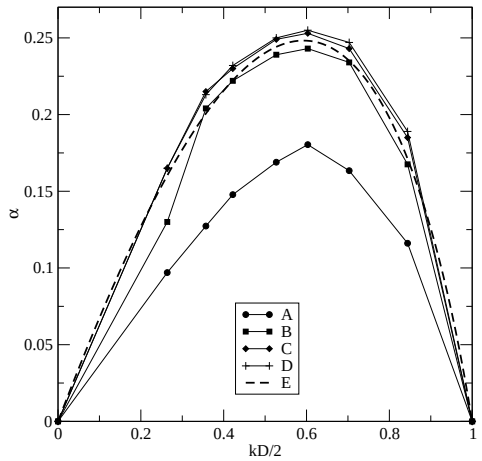

ρ_l	1000.	(Kg/m^3)	ρ_l/ρ_g	1000.
μ_l	$3.0 \cdot 10^{-3}$	$(Kg/m\,s)$	μ_l/μ_g	100.
σ	0.0725	(J/m^2)	Re_l	210.93
D	$0.633 \cdot 10^{-3}$	(m)	We_l	8.73
v_0	1.	(m/s)	Oh_l	0.014
λ	$3.5 \cdot 10^{-3}$	(m)	$k\,D/2$	0.57

Figure 3: Numerical growth rate α as a function of the adimensional wavenumber $k\,D/2$ for different viscosity ratios μ_l/μ_g (A:1, B:10, C:100, D:1000), compared to the inviscid theoretical curve (E). On the right the physical parameters of the numerical simulation of Fig. 4.

grid. The VOF interface at this level is very close to a front tracking representation with markers.

The phase structure is followed in time by solving an advection equation for the color function that is obtained by integrating (1) over the cell volume. The advection of the C data is a two-step procedure that requires the reconstruction of the interface in each cell. We consider a Piecewise Linear Interface Calculation (VOF/PLIC), followed by the calculation of the reference phase fluxes across the cell boundary to update the C value at the next time step. In axis-symmetric geometry we have implemented the ELVIRA reconstruction algorithm [8] with a geometrical unsplit area-preserving advection method [9]; in three dimensions we use the mixed Youngs-centered (MYC) reconstruction method followed by three split Lagrangian monodimensional advection steps [10]. The color function is advected at the fine level (f) and it is integrated over the coarse mesh to compute the density and viscosity distribution at level (c); the capillary force at the coarse level is obtained as the sum of the contributions at the fine level.

Results and Discussion

The stability of an infinitesimal amplitude wave on an initially axis-symmetric jet surface of infinite length has been studied with great detail by Yang for immiscible and inviscid fluids [11]. As a first test case we have analyzed this physical configuration with our numerical model that considers a liquid jet in a gas initially at rest. Physical properties of the liquid phase are $\rho_l = 1000\,Kg/m^3$ and $\mu_l = 0.01\,Kg/m\,s$, moreover $D = 0.633\,mm$, $\sigma = 0.0725\,J/m^2$, $\rho_l/\rho_g = 1000$ and variable viscosity ratio μ_l/μ_g. In Fig. 3 we show that as the gas viscosity decreases we recover the theoretical results of Yang. In that paper it is also shown that in the presence of an outer fluid when the Weber number $We = \rho_1 U_1^2 D/\sigma$ is greater than a critical number, $We > We_c$, asymmetric unstable modes can also develop. We consider now a pulsating jet with a sinusoidal oscillation of the inlet velocity, $v = v_0\,(1 + 0.5\sin(2\pi t/2.5))$. Physical

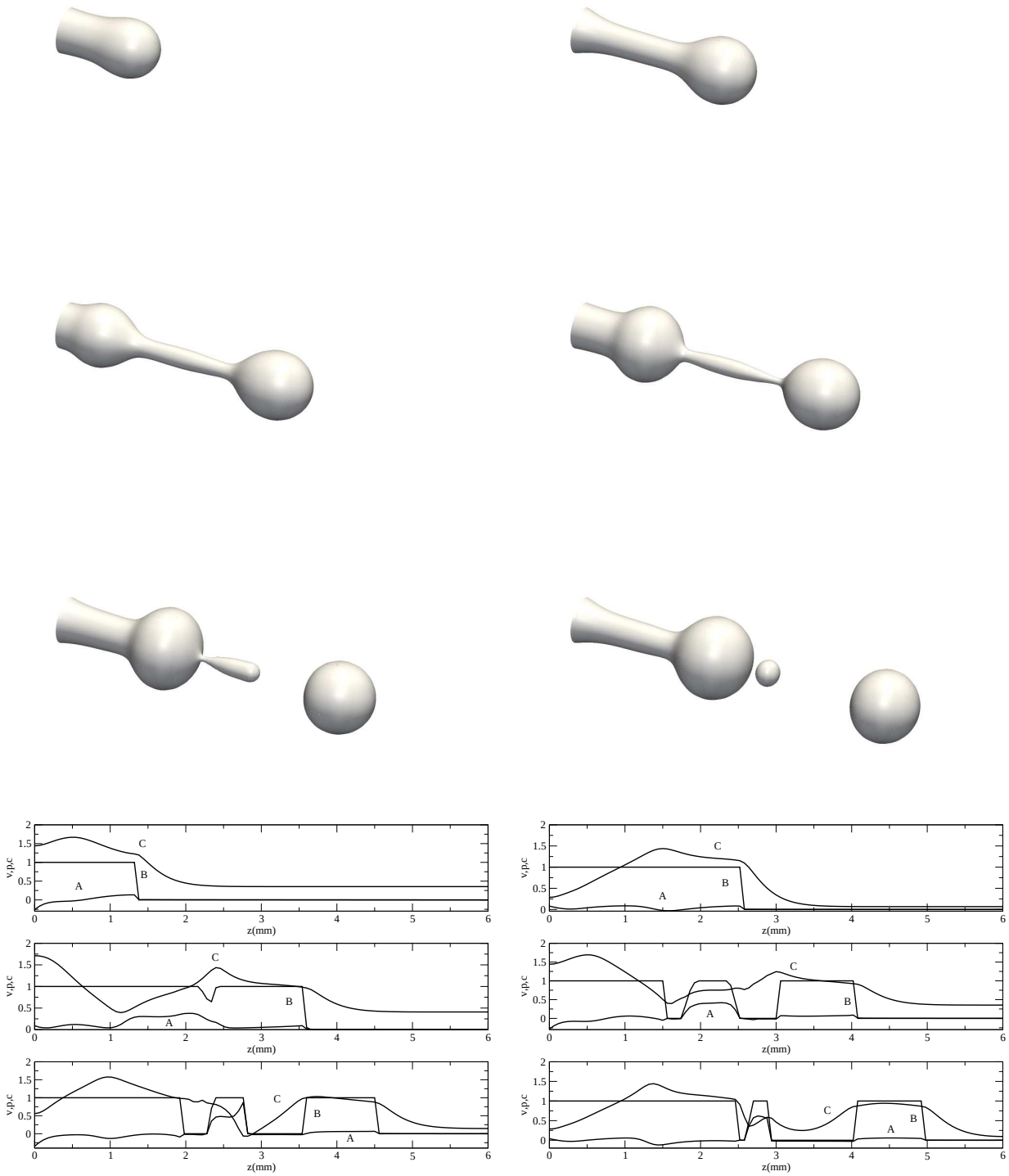

Figure 4: Jet evolution at nondimensional times $1., 2., 3., 3.5, 4., 4.5$ (top three rows from left to right) and pressure (A), color function (B) and velocity (C) profiles along the axis line at the same times (bottom three rows from left to right). The coarse resolution (c) has 64×384 cells with three levels of refinement ($f = c + 3$) for the color function.

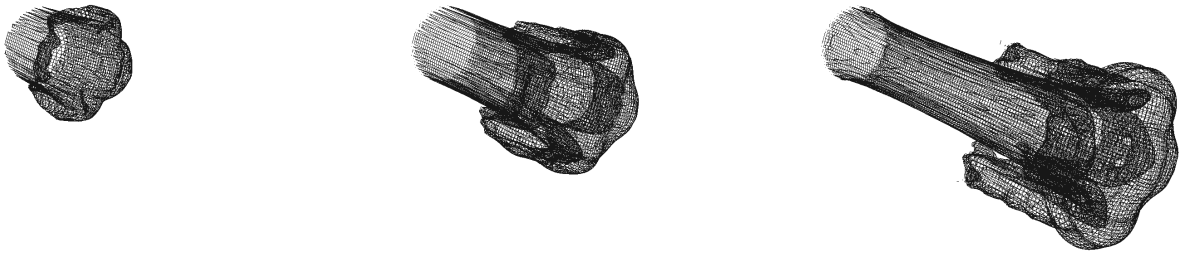

Figure 5: Three-dimensional simulation of the pulsating jet for $We > We_c$.

parameters for this simulation are given in Fig. 3 and the critical Weber number $We_c \simeq 1000$. The results of the axis-symmetric simulation are shown in Fig. 4. We observe the formation of a thread that first breaks in the front part and then in the back, forming a satellite droplet that becomes spherical under the action of surface tension. The breaking time is a function of the reconstruction algorithm and the fine grid resolution, as in any front capturing method. At a later stage of the simulation the satellite droplet merges with the incoming jet. After breakup, the main drop reaches a spherical shape as well, with a diameter about twice the jet diameter, in agreement with the experimental results [12]. By increasing the inlet velocity to $v_0 = 40\,m/s$, the Weber number, $We = 13968$, becomes bigger than the critical value and asymmetric modes develop at the jet surface, as shown in the three-dimensional simulation of Fig. 5.

Nomenclature

Ω	computational domain
Γ_s	interface
χ	phase indicator function
$\mathbf{u}, \mathbf{v}, \mathbf{w}$	velocity fields
p	pressure
$\mathbf{D}$	rate-of-strain tensor
$\mathbf{F}$	body force
$\mathbf{F}_s$	surface force
μ	viscosity
ρ	density
σ	surface tension
∇_s	surface gradient
R^{cf}	transfer operator
C	color function
Re	Reynolds number
We	Weber number
Oh	Ohnesorge number
D	jet diameter
k	wave number
Superscript	
f	fine level
c	coarse level
Subscript	
l	liquid phase (reference)
g	gas phase (secondary)
h	discretization

References

1. Scardovelli, R., and Zaleski, S., *Annu. Rev. Fluid. Mech.* 31:567-603 (1999).
2. Sussman, M.,Smereka, P., and Osher, S., *J. Comput. Phys.* 114:146-159 (1994).
3. Tauber, W., Unverdi, S.O., and Tryggvason, G., *Phys. Fluids* 14:2871-2885 (2002).
4. Landau, L.D., and Lifshiftz, E.M., *Mechanics*, Pergamon (1960).
5. Aulisa, E., Manservisi, S., and Scardovelli, R., *Comput. Methods Appl. Mech. Engrg.* 195:6239-6257 (2006).
6. Hysing, S., *Int. J. Numer. Meth. Fluids* 51:659-672 (2006).
7. Girault, V., and Raviart, P., *The Finite Element Method for Navier-Stokes Equations*, Springer, 1986.
8. Pilliod, J.E.Jr., and Puckett, E.G., *J. Comput. Phys.* 199:465-502 (2004).
9. Aulisa, E., Manservisi, S., Scardovelli, R., and Zaleski, S., *J. Comput. Phys.* 192:355-364 (2003).
10. Aulisa, E., Manservisi, S., Scardovelli, R., and Zaleski, S., *J. Comput. Phys.* 225:2301-2319 (2007).
11. Yang, H.Q., *Phys. Fluids A* 4:681-689 (1992).
12. Chaves, H., Obermeier, F., and Seidel, T., 8^{th} *ICLASS*, Pasadena, USA, 2000, pp. 1018-1025.